

## ● Original Contribution

# TISSUE CHARACTERIZATION OF PUBORECTALIS MUSCLE FROM 3-D ULTRASOUND

CATALIN CERNAT,<sup>\*,1</sup> SHREYA DAS,<sup>\*,1</sup> GIJS A.G.M. HENDRIKS,<sup>\*</sup> FRIEDA VAN DEN NOORT,<sup>†</sup>  
 CLAUDIA MANZINI,<sup>‡</sup> C. HUUB VAN DER VAART,<sup>‡</sup> and CHRIS L. DE KORTE<sup>\*,§</sup>

<sup>\*</sup> Medical Ultrasound Imaging Center (MUSIC), Radboud University Medical Center, Nijmegen, The Netherlands; <sup>†</sup> Robotics and Mechatronics, Technical Medical Center, University of Twente, Enschede, The Netherlands; <sup>‡</sup> Department of Reproductive Medicine and Gynecology, University Medical Center, Utrecht, The Netherlands; and <sup>§</sup> Physics of Fluids, Technical Medical Centre, University of Twente, Enschede, The Netherlands

(Received 29 March 2022; revised 27 September 2022; in final form 3 October 2022)

**Abstract**—Pelvic floor (PF) muscles have the role of preventing pelvic organ descent. The puborectalis muscle (PRM), which is one of the female PF muscles, can be damaged during child delivery. This damage can potentially cause irreversible muscle trauma and even lead to an avulsion, which is disconnection of the muscle from its insertion point, the pubic bone. Ultrasound imaging allows diagnosis of such trauma based on comparison of geometric features of a damaged muscle with the geometric features of a healthy muscle. Although avulsion, which is considered severe damage, can be diagnosed, microdamage within the muscle itself leading to structural changes cannot be diagnosed by visual inspection through imaging only. Therefore, we developed a quantitative ultrasound tissue characterization method to obtain information on the state of the tissue of the PRM and the presence of microdamage in avulsed PRMs. The muscle was segmented as the region of interest (ROI) and further subdivided into six regions of interest (sub-ROIs). Mean echogenicity, entropy and shape parameter of the statistical distribution of gray values were analyzed on two of these sub-ROIs nearest to the bone. The regions nearest to the bones are also the most likely regions to exhibit damage in case of disconnection or avulsion. This analysis was performed for both the muscle at rest and the muscle in contraction. We found that, for PRMs with unilateral avulsion compared with undamaged PRMs, the mean echogenicity ( $p = 0.02$ ) and shape parameter ( $p < 0.01$ ) were higher, whereas the entropy was lower ( $p < 0.01$ ). This method might be applicable to quantification of PRM damage within the muscle. (E-mail: [chris.dekorte@radboudumc.nl](mailto:chris.dekorte@radboudumc.nl)) © 2022 The Author(s). Published by Elsevier Inc. on behalf of World Federation for Ultrasound in Medicine & Biology. This is an open access article under the CC BY license (<http://creativecommons.org/licenses/by/4.0/>).

**Key Words:** 3-D ultrasound, Shape parameter, Puborectalis, Echogenicity.

## INTRODUCTION

The female pelvic floor (PF) muscles are a group of muscles that provide support of the PF organs and facilitate the passage of the baby during delivery (DeLancey 2016). This group of muscles is known as the levator ani muscles (LAMs). The puborectal muscle (PRM) is one of the LAMs. The PRM encircles the urogenital hiatus containing the PF organs such as the vagina, urethra and rectum, and it is attached on both sides to the bone pubic

symphysis (PS). PRM can stretch up to 250% of its original length during vaginal delivery (Svabík et al. 2009). This may cause permanent muscle trauma and represents a risk factor for later-life PF dysfunction such as pelvic organ prolapse (POP) and urinary or fecal incontinence (Silva et al. 2017). After vaginal childbirth, about half of all women present with substantial alteration of PRM function. PRM damage is currently the best-defined etiological factor in the pathogenesis of POP (Dietz 2013). Consequently, one-fourth to one-sixth of all women >40 years of age experience POP and urinary incontinence, respectively (Bedretdinova et al. 2016; Dieter et al. 2015). This is associated with major inconveniences in their daily life (van de Waarsenburg et al. 2019).

Ultrasound (US) imaging is already used as a diagnostic tool to detect avulsion of the PRM resulting from

Address correspondence to: Chris L. de Korte, Medical Ultrasound Imaging Center, Department of Medical Imaging, Radboud University Medical Center, PO Box 9101 (766), Geert Grooteplein Zuid 10 (767), 6500 HB Nijmegen, The Netherlands. E-mail: [chris.dekorte@radboudumc.nl](mailto:chris.dekorte@radboudumc.nl)

<sup>1</sup> These authors contributed equally.

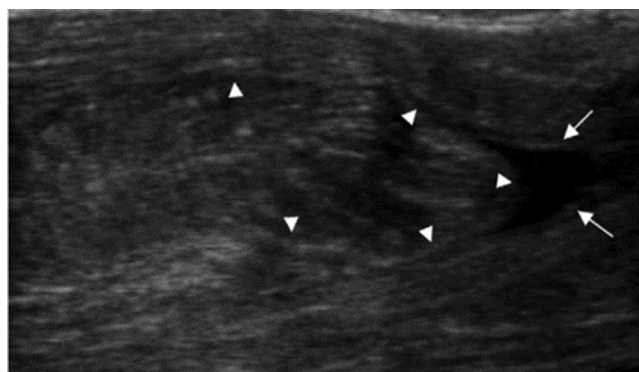


Fig. 1. Rectus femoris showing partial tears (*arrowheads*) and a small hematoma (*arrows*). Permission has been granted by the publisher to use this image (Woodhouse and McNally 2011).

muscle trauma, which may lead to POP (Dietz 2013). Furthermore, the irreversible overdistension of the levator hiatus can also be diagnosed by measuring the levator hiatal area during Valsalva maneuver. Van de Waarsenburg et al. (2019) and Grob et al. (2018) reported that there are changes in the mean echogenicity (MEP) and levator hiatal area after vaginal delivery using 2-D US images. Grob et al. (2018) report that tomographic ultrasound imaging was performed on volumes obtained on maximum pelvic floor muscle contraction (PFMC) at 2.5-mm slice intervals, from 5 mm below to 12.5 mm above the plane of minimal hiatal dimensions (eight slices). Strain measurement was performed on the slice of minimal hiatal dimensions, that is, the tomographic US image (TUI) slice in which the pubic bones are closed. This means that one 2-D slice was selected from these eight slices within the volume at rest and the volume at contraction. A similar method was also used by the authors from the article by van de Waarsenburg et al. (2019). Three-dimensional quantitative US (QUS) analysis takes into account the entire muscle rather than a partial muscle in 2-D slices. It enables us to analyze differences between parts within the PRM, leading to a better understanding of this PF muscle and the trauma it causes.

#### *Muscle trauma/damage in US images*

As presented by Woodhouse and McNally (2011), strains, tears and lacerations are muscle injuries most commonly caused by over-elongation of muscles in the body. These indirect muscle injuries have altered microstructural composition. In US imaging, US waves are absorbed, reflected or scattered by structures in the human body. The brightness of the pixels in a B-mode US image depends on the strength of the returning echo (van Holsbeeck and Introcaso 2001; Whittaker and Stokes 2011). Echogenicity or mean echogenicity (ME) is the average of this brightness of the pixels or the gray

values (gray scale with a range of 0–255) of the pixels of an object in a B-mode US image. The microstructural composition of muscle tissue can be assessed indirectly by measuring the echogenicity or reflective properties of the tissue (Bellos-Grob 2016). Muscle injuries can be visualized in a US image as areas of altered echogenicity within the muscle. Figure 1 illustrates a partial tear of muscle fibers of the rectus femoris (located in the upper leg) and a small hematoma (Woodhouse and McNally 2011).

Recurrent and/or severe muscle injury, on the other hand, can leave behind intramuscular scars, which appear as hyper-reflective foci or hyper-echogenic areas. These injuries can alter the functional dynamics of the surrounding muscle (Woodhouse and McNally 2011). Such an example of a hyper-echogenic region resulting from muscle injury can be seen in Figure 2 (Woodhouse and McNally 2011).

Muscle damage to LAMs can be microscopic leading to changes in microstructural composition or macroscopic damage. One of the most common forms of macroscopic damage of the LAMs is known as avulsion. Avulsion of the PRM can be unilateral or bilateral. In cases of unilateral avulsion, the disconnection of PRM is from one side of the bone PS, whereas in cases of bilateral avulsion, disconnection is from both sides of the PS.

#### *Diagnosis of muscle damage in LAMs*

Unilateral or bilateral avulsion can be diagnosed according to Dietz (2010) by palpation or digital assessment of the PF muscle (PFM) via the vaginal or transanal route. However, this method poses a challenge as the clinician must be trained to diagnose it correctly. Furthermore, the distinction between partial or complete trauma can be hard to detect (Dietz 2010).

The alternative, more reproducible way of diagnosing such trauma is with the aid of US imaging. The use of 3-D or 4-D transperineal US (TPUS) to render

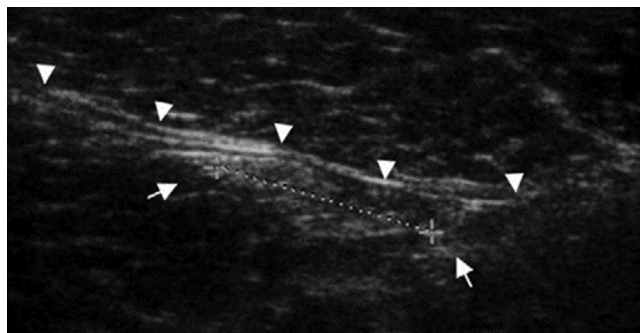


Fig. 2. Scar formation (*arrows*) seen after recurrent injury, adjacent to the muscletendinous junction (*arrowheads*) at the site of the original injury. Permission has been granted by the publisher to use this image (Woodhouse and McNally 2011).

volumes was first described in 2004 (Dietz 2010). Using these volumes, the clinician evaluates by assessing different inter-slice intervals (2-D images within a certain volume) containing the PRM. Diagnosis of unilateral avulsion is performed by measuring the distance of each end of the insertion point of the PRM from the urethra in the 2-D images. If this distance is  $>25$  mm for one of the ends, it is considered to be disconnected from its insertion point, the PS (Dietz 2010). Hence the diagnosis is unilateral avulsion.

Avulsion of the PRM from the bone can occur with or without microdamage within the muscle. This microdamage could be indicative of the extent of damage of the PRM, even if this is not revealed by the apparent symptoms or, more importantly, through primary observation of TPUS images. This is due to the fact that in B-mode US, only the macrostructures are imaged and the microstructures, such as scar tissue, within the PRM are difficult to image without using computational methods (van Hooren *et al.* 2020).

#### *Aim of the study*

The aim of this study was to develop a quantitative ultrasound (QUS) tissue characterization method to obtain diagnostic information on PRMs with and without avulsion. We hypothesized that the presence of an avulsion of the PRM results in a change in the statistical distribution of gray values in a B-mode US image of the PRM.

We performed this study to investigate whether QUS parameters differ between PRMs without avulsion and PRMs with unilateral avulsion. Women with PRMs without damage are nulliparous women, which means there is no damage caused by vaginal childbirth. Women with unilateral avulsion are non-nulliparous, and because avulsion is present, they have some form of damage within the PRM. Most women who are non-nulliparous and undergo vaginal delivery exhibit some form of PRM damage (Dieter *et al.* 2015; de Araujo *et al.* 2018). Furthermore, two distinct scenarios were analyzed: first,

when the muscle was at rest, and second, when the muscle was voluntarily contracted. The accuracy of the QUS method developed is then evaluated based on its ability to distinguish between damaged and undamaged PRM using the receiver operating characteristic curve (ROC).

## METHODS

#### *Data acquisition*

Three-dimensional/four-dimensional (3-D/4-D) TPUS was acquired using Philips X6-1 matrix transducer connected to an EPIQ 7G US machine (Philips Healthcare, Bothell, WA, USA), at the University Medical Centre (UMC), Utrecht, the Netherlands. Data was acquired from the PRMs in women without an avulsion ( $n_1 = 8$ ) and in women with unilateral avulsion ( $n_2 = 6$ ). The Medical Research Ethics Committee of UMC Utrecht exempted the project from approval, and all volunteers signed informed consent forms.

All the data from women with undamaged as well as unilateral avulsion of the PRMs were acquired with the same pre-set in the US machine. The time-gain compensation (TGC) and other settings such as filtering, contrast, gain, power, gray map and processing were identical for all acquisitions. Because the US machine and the matrix transducer were identical for all acquisitions, the B-mode log compression, normalization, and so on were also the same. That is why two different scans for the same woman/subject will not reveal different levels of brightness. Two different scans from different women/subjects will reveal similar or different levels of echogenicity regarding differences in the state of the tissue. Furthermore, as the same clinician acquired all the data, inter-observer variability is also eliminated.

In each of the acquired data sets, one volume consists of  $352 \times 229 \times 277$  pixels (in the x-, y- and z-directions respectively). The physical size of the volume is  $14.78 \times 13.74 \times 9.41$  cm. The volumetric data were acquired at the rate of approximately 1.5 vol/s resulting in 22 volumes that span over 11–15 s. The data were

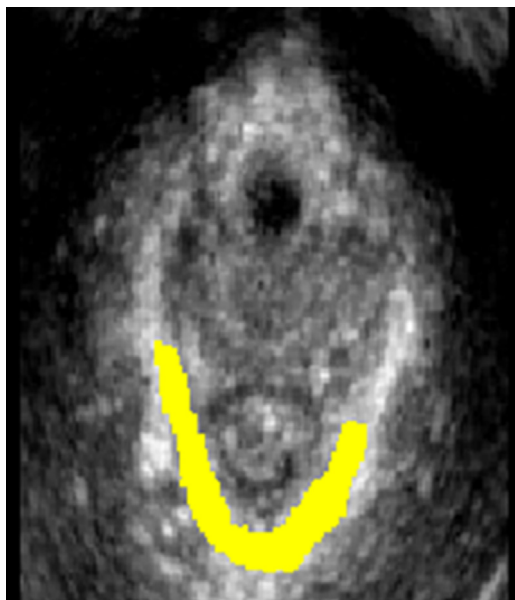


Fig. 3. Slice of an ultrasound volume of a puborectalis muscle (top view).

stored in Digital Imaging and Communications in Medicine (DICOM) format. In [Figure 3](#), a slice of the 3-D volume containing the PRM can be seen. The *yellow highlighted area* represents the PRM.

During data acquisition, the women voluntarily contracted their PF muscles from rest to maximum contraction. Based on the principle of altered echogenicity caused by muscle trauma, [Crema et al. \(2015\)](#) presented a new approach to detecting minor muscle injuries. In dynamic ultrasound assessment, the candidate voluntarily contracts the muscle to better expose areas of low echogenicity inside the muscle. These areas could be minor partial tears or minor strains of muscle fibers. These partial tears or minor strains appear as ill-defined hypo-echogenic areas at rest, whereas in contraction these appear as much more prominent areas of low echogenicity. This was analogous to our situation, as the women voluntarily contracted their PRMs starting from rest.

#### Muscle segmentation and ROIs

The PRM was segmented in the 3-D volume at rest as described by [Manzini et al. \(2021\)](#). [Van den Noort et al. \(2018\)](#) reported that automatic segmentation provides volumes similar to those provided by manual segmentation of the PRM. For the purpose of this work, the segmented PRM at rest was used. The 3-D volume of the segmented muscle can be seen in [Figure 4](#).

The segmented volume of the muscle at rest ([Fig. 4](#)) was tracked over the contraction cycle by estimating inter-volumetric displacements. Each of the 3-D US volumes contained  $352 \times 229 \times 277$  ( $X \times Y \times Z$  in



Fig. 4. Three-dimensional volume of segmented puborectalis muscle at rest.

Cartesian coordinate system) pixels, which were uniformly sampled at distances of  $0.42 \times 0.60 \times 0.34$  mm (non-uniform intervals  $dx \times dy \times dz$ ). For each pair of subsequent volumes using a 3-D normalized cross-correlation algorithm ([Hendriks et al. 2016](#); [Gijbertse et al. 2017](#); [Das et al. 2021](#)). In this algorithm, two subsequently recorded volumes were subdivided into 3-D blocks called *kernels* and *templates*. The kernels were matched on the templates, and the locations of the 3-D cross-correlation peaks were calculated. These locations of peaks indicated the displacements between the two blocks. To estimate subsample displacements, the cross-correlation peaks were interpolated (parabolic fit). The displacement estimates were finally filtered using a 3-D median filter. For each inter-volume displacement estimate, the position of the muscle was tracked by accumulating all the previous displacement estimates up to the current time point. The resulting segmentation from tracking made it possible to also analyze the PRM in the contracted state. Henceforth, the 3-D segmentation of the PRM, both at rest and in contraction, is referred to as the 3-D mask.

Initially, the US grid (or coordinates) specifies the indices and their corresponding B-mode gray values of the entire 3-D volume, including the indices of the muscle at rest. This is the initial 3-D mask at rest. When the muscle is contracted and deformed, the indices at rest are tracked or followed in the same US grid to the now displaced indices. This is each 3-D mask in contraction. Thus, the US grid or coordinates do not change over time, but the indices of the muscle change spatially within the fixed coordinates, and these are spatial coordinates or a Eulerian description ([Mase et al. 2010](#)). Furthermore, the reference coordinates we have for each volume and thus the 3-D mask are Cartesian, as is the rectilinear coordinate system (non-uniform intervals  $dx$ ,  $dy$  and  $dz$  for x-, y- and z-axes, respectively).

The 3-D mask of the PRM for both rest and contraction volumes had first been used for dividing the muscle into two parts with approximate equal volumes. This had been done by calculating the length of the opening



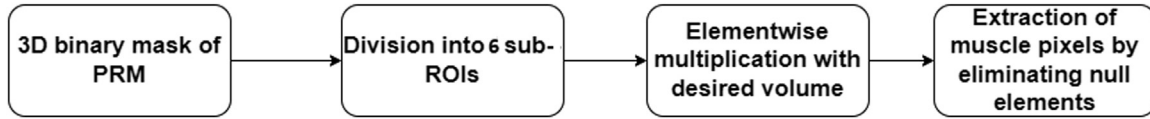


Fig. 5. Process of division of the segmented puborectalis muscle (PRM) into subregions of interest. ROI = region of interest

between two ends of the PRM (in x-axis) and dividing this length to obtain the midline of the muscle, from the top view. Thereafter, for each of these two parts separated by the midline, three equal divisions are calculated (in the z-axis). Thus, the total muscle is divided into approximately six equal parts. While dividing the muscle into parts, the corresponding y-axis indices are not used because the y-axis represents the thickness of the muscle. In other words, each of the sub-ROIs had the complete thickness of the muscle. These 3-D indices were saved as a binary mask (having 0 or 1 values), for both rest and contraction. The gray values were extracted by multiplying each sub-ROI by the US volume, in 3-D. This process is illustrated in Figure 5.

Unilateral avulsion of a PRM results in a disconnection from one end of the PS, whereas in a PRM without avulsion, both ends are connected to the PS. To better exploit this detail, the muscle was divided into six regions of interest (sub-ROI 1 to sub-ROI 6) as illustrated in Figure 6a and in the block diagram. The muscle was divided into six sub-ROIs to make this method applicable to any number of woman. As PRMs have been found to vary in length and volume from woman to woman, each muscle was subdivided after calculating its particular length (in x-axis) and depth (in z-axis). In this way, the two ends nearest the bone were kept as one-sixth of the total volume of the muscle, in terms of number of indices or pixels in 3-D. This can be seen in the example in Figure 6b.

The clinical reason for choosing the two endpoints of the PRM is that the damage to the PRM is likely to be present near the location of disconnection from the bone. Moreover, because of the complex shape of the PRM, there are parallel and perpendicular fibers with respect to the US transducer. Regions of the muscle that is connected to the PS have a parallel fiber orientation, whereas in the midregion, the fiber orientation is perpendicular to the US transducer as confirmed by MR tractography (Zijta *et al.* 2013). This difference in orientation would further have different backscattering from different regions of the muscle (Holland *et al.* 1998). As the two regions nearest the bone have parallel muscle fibers, they are comparable.

#### Mean echogenicity

Grob *et al.* (2018) found that structural changes in the muscle can be distinguished and analyzed by measuring the mean echogenicity (ME) of the PRM, during and after pregnancy. It was found that 6 months postpartum, the ME was significantly lower ( $p < 0.001$ ) than during pregnancy. Therefore, it is expected that structural changes caused by muscle trauma can also be analyzed using ME. In this study, ME was calculated by summing the gray values of the pixels in each sub-ROI and dividing the result by the number of pixels in that sub-ROI,

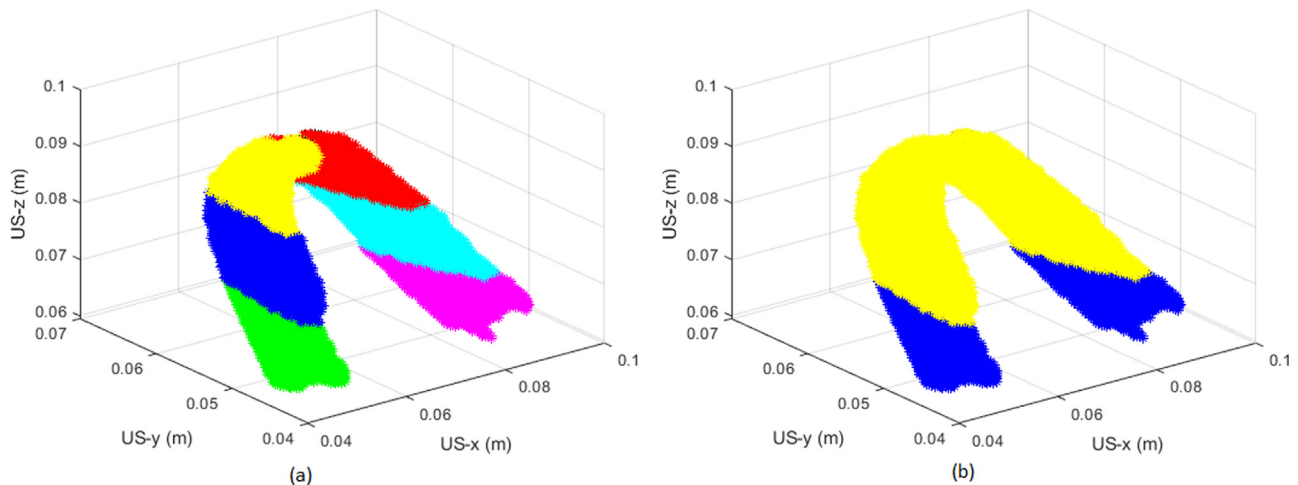


Fig. 6. (a) Subregions of interest of puborectalis muscle after division. (b) Two subregions nearest the insertion points at the pubic bone. US = ultrasound.

$$ME = \sum_{i=0}^m \sum_{j=0}^n I(i,j) \quad (1)$$

where  $I(i, j)$  is the gray value of the pixel at location  $(i, j)$  from the region of interest of size  $m * n$  pixels, where  $m$  and  $n$  are the corresponding 2-D directions. In our case, the gray value for each 3-D index was divided by the number of indices in that region.

#### Shannon's entropy

Shannon's entropy is a widely used QUS technique for US tissue characterization that measures the signal uncertainty or level of information. [Chen et al. \(2020\)](#) investigated the clinical value of Shannon's entropy in grading different stages of hepatic steatosis. The results were compared with those of a deep learning VGG-16 model. It was determined that Shannon's entropy outperformed VGG-16 in identifying candidates with moderate or severe hepatic steatosis. Furthermore, the authors determined that when compared with a conventional statistical parametric method based on the Nakagami distribution, Shannon's entropy outperformed it with a 10% higher area under the receiver operating characteristic (ROC) curve. For a given ROI, Shannon's entropy can be calculated as described by [Chen et al. \(2020\)](#),

$$H_c = - \sum_{i=1}^n w(y_i) \log_2 [w(y_i)] \quad (2)$$

where  $w(y_i)$  represents the probability value obtained from the normalized histogram counts,  $n$  is the number of bins in the histogram and  $y_i$  is the discrete random variable of the backscattered echo intensity.

In our case, because we have used gray scale values from B-mode images,  $w(y_i)$  denotes the probability of a gray scale value  $y_i$  that is present within the ROI. The smaller the probability of a gray scale value  $y_i$  being present, the higher is the level of information of this gray scale value and vice versa.  $H_c$  is the sum of all possible gray scale values from 1 to  $n$ . Values of  $H_c$  range from 0 (low level of information) to infinity (high level of information). Thus,  $H_c$  measures the granularity of a region. A homogeneous region has a low level of information and, thus, low entropy, whereas a more granular region has a higher level of information and, thus, higher entropy ([Gdynia et al. 2009](#)).

It is expected that a change in the structure of the PRM would result in a change in the entropy, leading to the change in the level of information that a region within the PRM may contain.

#### Statistical distribution of gray values

As mentioned by [Girardi \(2019\)](#), tissue microstructure information can be found in the envelope of the

backscattered ultrasonic echo. The envelope of the backscattered ultrasonic echo from tissues is dependent on the shape, size and density of the scatterers inside the tissue ([Tsui et al. 2010](#)). According to statistics on US echoes measured from biological tissues, the envelope can be classified as a pre-Rayleigh, Rayleigh or post-Rayleigh distribution. All these three types of distributions can be modeled by the Nakagami distribution. The probability distribution of the Nakagami model is given by ([Tsui et al. 2010](#)),

$$p_a(A | \Omega) = \frac{2m^m A^{2m-1}}{\Gamma(m)\Omega^m} * \exp\left(\frac{-mA^2}{\Omega}\right) * U(A) \quad (3)$$

where  $U(A)$  is the unit step function,  $\Gamma(m)$  is the gamma function,  $A$  corresponds to possible values of the random variable of the backscattered signal envelopes,  $m$  is the Nakagami shape (or spread) parameter and  $\Omega$  is the scaling factor.

If the envelope follows a Nakagami distribution, then the intensity follows a gamma distribution ([Sikdar et al. 2018](#)), and the probability density function (PDF) is given by,

$$P_{\text{Gamma}}(I | \alpha, \beta) = \frac{\beta^\alpha}{\Gamma(\alpha)} I^{\alpha-1} e^{-\beta I} \quad (4)$$

where  $\Gamma(\alpha)$  is the gamma function,  $I$  is the intensity of the US backscattered signal,  $\alpha$  is the shape parameter and  $\beta$  is the rate parameter.

The shape parameter of the gamma distribution results from the pixel distribution within each ROI of the B-mode image of the PRM. It was determined using a maximum likelihood estimator.

It is expected that a change in the tissue microstructure would be reflected in a change of the pixel distribution in each ROI, resulting in a change in the shape parameter as well.

#### Analysis procedure

In analysis of an undamaged PRM, both sub-ROI 1 and sub-ROI 6 were used, while for a PRM with unilateral avulsion, either sub-ROI 1 or sub-ROI 6 was used. This was based on whether the avulsion was located on the left (sub-ROI 1) or on the right (sub-ROI 6). To analyze the regions closest to possible damage, the regions closest to the insertion points were considered.

The mean echogenicity, entropy and shape parameter values of the gamma distribution were computed for each sub-ROI at rest and in maximum contraction. As the sample size was small, the Wilcoxon rank sum test was used to determine whether the computed values could be described by distributions with equal medians. Equal medians would imply that the proposed parameters cannot be used to distinguish damaged from

undamaged PRMs. Alternatively, a lower  $p$  value, indicating that the computed values are from distributions with unequal medians, would imply that the proposed parameters can be used to distinguish damaged from undamaged PRMs.

Furthermore, for each parameter, the receiver operating characteristic (ROC) curve was computed and the area under the curve (AUC) was calculated to compare the diagnostic ability of a classifier using each of the three parameters described previously. The ROC curve is created by plotting the true-positive rate (TPR) against the false-positive rate (FPR) at various threshold settings (Cardillo 2021).

## RESULTS

In Figure 7 are the results for ME, entropy and shape parameter values illustrated as adjacent boxplots comparing PRMs with and without avulsion both at rest and in maximum contraction. On each boxplot, the central mark indicates the median, and the bottom and top edges of the plots indicate the 25<sup>th</sup> and 75<sup>th</sup> percentiles, respectively. The whiskers extend to the most extreme data points not considered outliers. The outliers are plotted individually using the + symbol (MATLAB version R2021a, 2021, The MathWorks Inc., Natick, MA, USA).

The statistical criterion used to determine an outlier is the one used as the default in MATLAB. By default, an outlier is a value that is more than three scaled median absolute deviations (MADs) away from the median.

In Figure 8 are the exact ROC curves for the mean echogenicity, entropy and shape parameter values as adjacent lineplots comparing PRMs at rest and in maximum contraction.

### Mean echogenicity

When PRMs were at rest, the ME was increased ( $p < 0.01$ ) for PRMs with unilateral avulsion compared with PRMs without avulsion. The distance between the medians of the two classes was found to be 34.69, and the AUC was 0.94. This means that it is possible to correctly distinguish damaged from undamaged PRMs with the help of ME, with a probability of 94%, when calculated at rest.

For PRMs in contraction, the ME did not increase ( $p = 0.75$ ) for PRMs with unilateral avulsion compared with PRMs without avulsion. Thus, it can be said that ME in contraction is not effective in distinguishing damaged from undamaged PRMs. The distance between the medians of the two classes was found to be 2.42. As there is almost no difference between the two groups, ROC analysis revealed an AUC of 0.56.

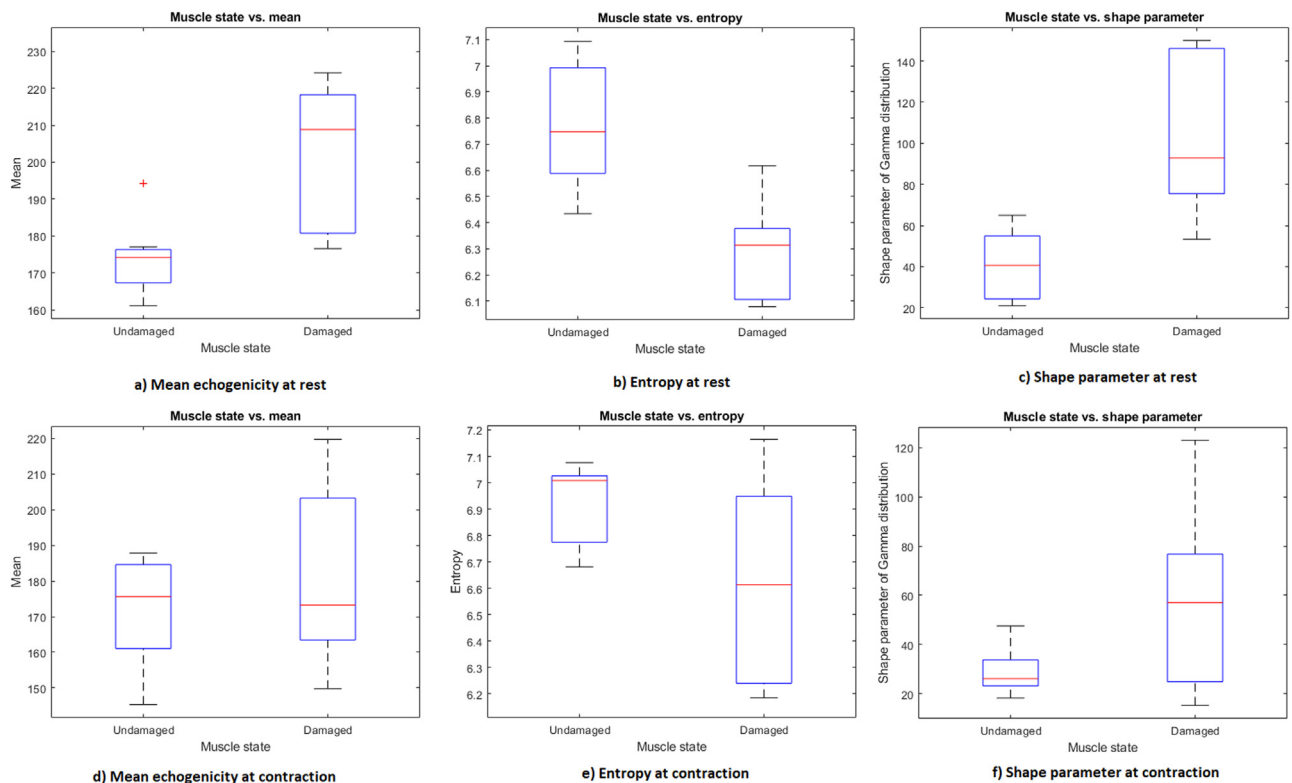


Fig. 7. Mean echogenicity, entropy and shape parameter values for the puborectalis muscle without avulsion and with unilateral avulsion, at rest (*top row*) and in contraction (*bottom row*).

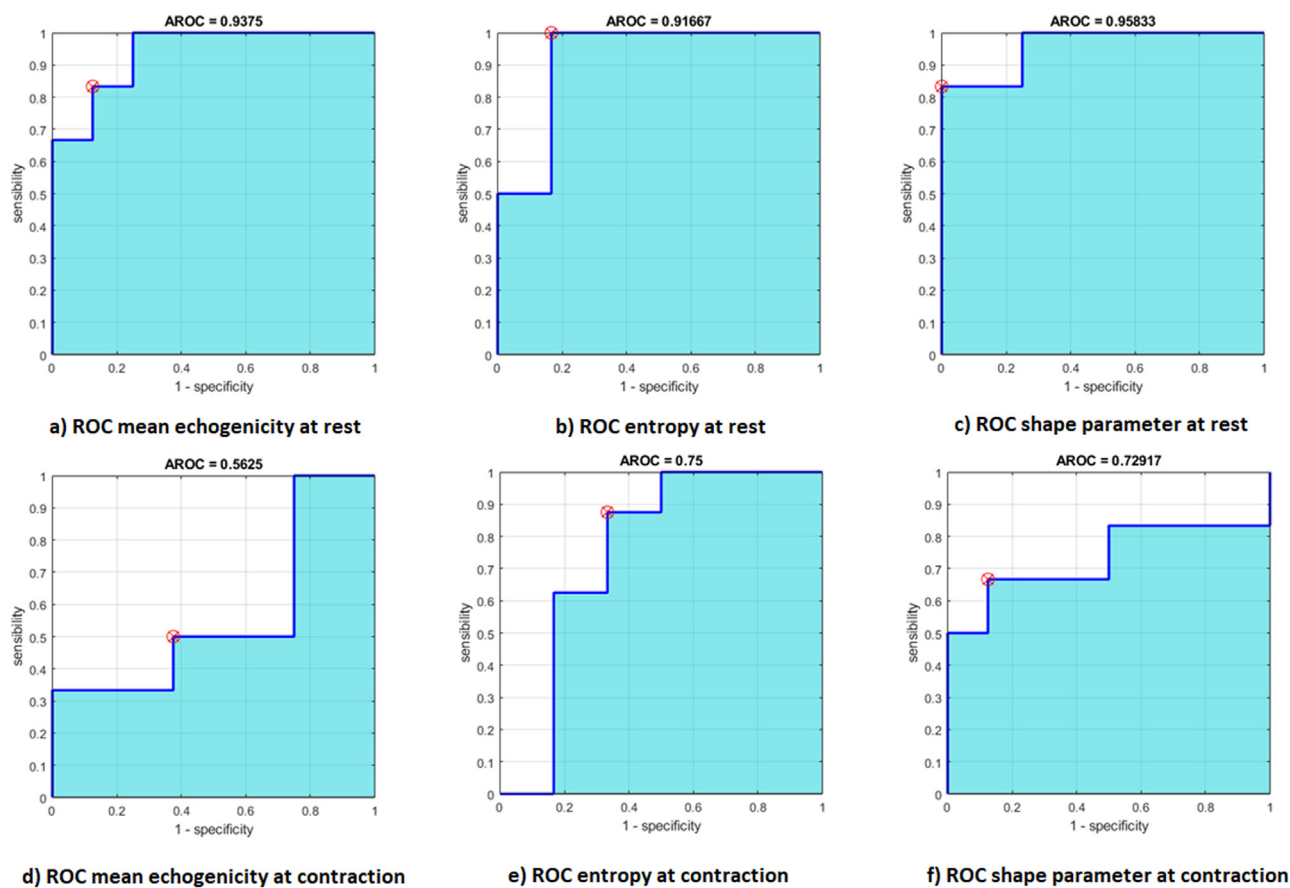


Fig. 8. Receiver operating characteristic (ROC) curves for mean echogenicity, entropy and shape parameters when puborectalis muscles were at rest (*top row*) and in contraction (*bottom row*). Here the *blue area* represents the area under the ROC (AUC), and the *red points* represent the discrete values.

### Entropy

When PRMs were at rest, the entropy exhibited a decrease ( $p < 0.01$ ) for PRMs with unilateral avulsion compared with PRMs without avulsion. The distance between the medians of the two classes was found to be 0.43 and the AUC was 0.89. The high AUC value indicates that there is a probability of 89% of correctly distinguishing a damaged PRM from an undamaged one when using entropy values calculated at rest.

For the PRMs in contraction, entropy did not exhibit a significant decrease ( $p = 0.14$ ) for PRMs with unilateral avulsion compared with PRMs without avulsion. The distance between the medians of the two classes was found to be 0.39 and the AUC was 0.75.

### Shape parameter of gamma distribution

When PRMs were at rest, the shape parameter value exhibited an increase ( $p < 0.01$ ) for PRMs with unilateral avulsion compared with PRMs without avulsion. The distance between the medians of the two classes was found to be 52.19, and the AUC was 0.96.

For the PRMs which were in contraction, the shape parameter did not significantly increase ( $p = 0.28$ ) for PRMs with unilateral avulsion compared with PRMs without avulsion. The distance between the medians of the two classes was found to be 30.98 and the AUC was 0.73. Similar to ME and entropy, the AUC for the shape parameter is also smaller in contraction.

The summarized results for the distance between the medians, the statistical significance and the AUC for the fitted and exact curves for each parameter can be found in [Table 1](#) for PRMs at rest and in contraction.

Furthermore, images with representative colors were created by assigning each ROI within the PRM the value of the shape parameter. These images can provide a visual aid to the clinician in diagnosing the disconnected ends of the PRMs closest to the insertion points. In this way, information regarding the locality of the damage within the PRM was visualized. Such an example can be seen in [Figure 9a](#) and [9b](#), where *blue* corresponds to low values of the shape parameter which indicate regions of undamaged tissue, whereas *yellow*



Table 1. Results for the three parameters at rest and contraction

	State of puborectalis muscle					
	At rest			In contraction		
	Mean echogenicity	Entropy	Shape parameter	Mean echogenicity	Entropy	Shape parameter
Distance between medians	34.69	0.43	52.19	2.42	0.39	30.98
Statistical significance ( <i>p</i> value)	<0.01	<0.01	<0.01	0.76	0.14	0.18
AUC fitted curve	0.91	0.89	0.93	0.52	0.75	0.73
AUC exact curve	0.94	0.92	0.96	0.56	0.70	0.73

AUC = area under the receiver operating characteristic curve.

corresponds to high values of the shape parameter indicating regions of damaged tissue.

## DISCUSSION

In this article, we have described a method for QUS analysis of damaged and undamaged PRM to distinguish between avulsion and non-avulsion. The principal finding of the study is that the echogenicity, entropy and shape parameters investigated for the avulsion group differ from those for the non-avulsion group when the PRM is at rest. In women without avulsion, the echogenicity-based parameters of the two sides of the PRM are similar at rest.

In contraction, all parameters performed worse in differentiating damaged from undamaged PRM. During contraction, although the tissue composition does not change, the muscle fibers contract, which results in a different backscattering of the US waves with respect to the rest situation (Rijsterborgh *et al.* 1990; Holland *et al.* 1998).

## Physical interpretation

Van de Waarsenburg *et al.* (2019) investigated the structural composition of PRM before and after delivery. It was found that ME significantly increased from 1 day to 24 weeks after delivery. The authors studied this using 2-D images of the levator hiatus in an axial position and minimal hiatal area. This is in line with our finding that ME increases for the damaged PRM at rest. Furthermore, instead of one slice from the volumetric data, we used the entire PRM, automatically segmented. The increase in ME means that the brightness of the region has increased which might be the result of connective tissue formation in damaged PRMs. ME is lower for undamaged PRM, which indicates the absence of connective tissues.

Our finding that in contraction the echogenicity of the avulsed regions is decreased is in line with fundamental studies performed at the myocardial wall. Integrated backscatter, a normalized parameter representing echogenicity, is decreased in the myocardium during systole compared with diastole (Rijsterborgh *et al.* 1990). In systole the cardiac muscle is thickened with

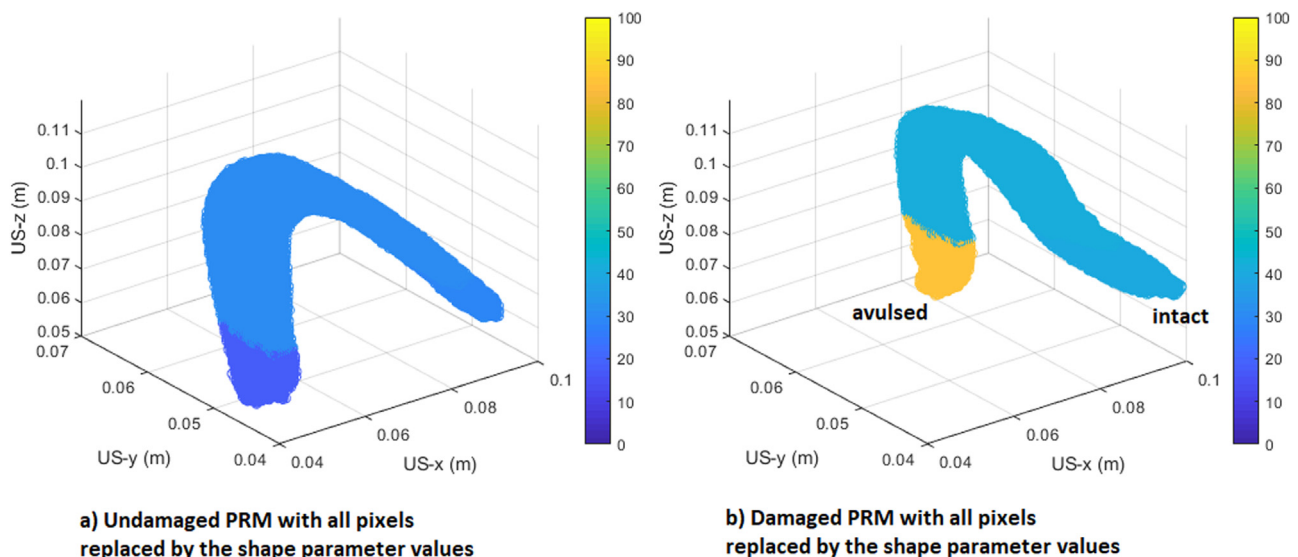


Fig. 9. Visual representation of the shape parameter change for (a) an undamaged and (b) a damaged puborectalis muscle (PRM) at rest. US = ultrasound.

respect to diastole, which is perfectly in line with our finding that in contraction, the echogenicity of the avulsed part is decreased.

As the information content of a region in an image is known as entropy, a homogeneous region would have lower entropy and an inhomogeneous or granular region would have higher entropy. From our results, entropy was decreased for PRMs with unilateral avulsion compared with PRMs without avulsion, at rest. This could indicate that the entire region has a homogeneous formation of scar tissue throughout the muscle, which has replaced the muscle fibers. Thus, the normal muscle tissue with echogenicity determined by the orientation of the fibers would still have more entropy or granularity than PRM with unilateral avulsion, especially because we have always considered the end of the muscle, which is disconnected, as likely to contain scar or connective tissue.

Lastly, our results indicated that there was a change in the tissue microstructure depicted by the shape parameter. The shape parameter was lower for undamaged PRMs and higher for the damaged PRMs, at rest. The shape parameter follows a Rayleigh distribution according to different scatterer concentrations in the tissue. It moves from a pre-Rayleigh to a Rayleigh distribution if the tissue distribution becomes more homogenous (and vice versa) (Weng et al. 2017). Thus, if the scar or connective tissue formation in the disconnected region of the damaged PRMs is homogeneous, this would lead to an increase in the shape parameter in damaged as compared with undamaged PRMs. This is also consistent with the results obtained for the damaged PRMs with lower entropy and higher echogenicity as compared with undamaged PRMs.

Our finding that microstructural damage of the PRM might be made visible using the method described in this research has the potential to become of clinical relevance as an early indicator of possible avulsion/later-life disorders. Such a use could occur when a woman would like to have a second childbirth and the US image of the PRM is analyzed using the shape parameter. If the muscle is found to have microstructural damage, then the clinician could estimate whether it is going to become avulsed after childbirth. However, thorough validation of this method on a larger data set containing women with or without known damage of the PRM is required to determine if the algorithm can reliably aid the clinician in the diagnosis of microstructural damage.

#### *Limitations and shortcomings*

One main limitation and two shortcomings of the method have been identified. The limitation is that the number of the data sets ( $n = 14$ ) was small, which resulted in the use of a non-parametric test for

evaluation. This limits the techniques that could be used to rather conventional as opposed to more modern, machine learning/deep learning-oriented techniques. However, even though this study involved a small number of patients and used a non-parametric test, a significant difference between undamaged and avulsed tissue was found for the three parameters investigated. Furthermore, the age of the women was unknown, and therefore, whether age has any influence on the structure of the muscle could not have been accounted for.

A shortcoming is that different US machines and transducers provide unique B-mode images. It makes the application of this method machine dependent as different machines use different transmitter frequencies, transducer sensitivities, beam profiles, signal-to-noise ratios and so on, resulting in different echograms. This limits direct translation of our findings to other machines and centers. To overcome this shortcoming, a comparison of the echogenicity using phantoms can be done using matrix transducers for different commercially available US machines. Thereafter, factors by which the echogenicity might change can be calculated and applied to have comparable measurements (Thijssen et al. 2008; Weijers et al. 2012, 2016).

The second shortcoming is that although the methods proposed can distinguish between PRMs with and without avulsion relative to each other, no conclusion can be drawn regarding the type of damage/trauma with which each muscle is affected. The increase in the ME of the PRMs with unilateral avulsion, at rest, might indicate scar tissue formation, although this conclusion cannot be drawn from this measurement alone. This shortcoming can be overcome by calculating functional parameters such as strain to determine differences in contractility between undamaged and damaged muscles (Das et al. 2021).

Furthermore, although Dieter et al. (2015) indicate that high-frequency linear array probes,  $>7$  MHz and preferably  $>10$  MHz, are required to adequately image muscle, a 1- to 6-MHz matrix probe was used. This is because increased spatial resolution (achieved through higher US frequencies) comes at the cost of decreased penetration depth limiting the ability to image deeper located structures (van Holsbeeck and Introcaso 2001). Therefore, it was crucial that depth penetration was ensured so that the PRM could be imaged completely. Furthermore, the number of elements has to be increased to obtain a similar field of view when using high frequency.

#### *Future directions*

The results obtained in this article illustrate the potential of quantitative echography to identify PRM avulsion. The different parameters could serve as input

(a so-called feature) for more specialized machine learning algorithms such as neural networks. However, it is crucial for such applications that the data set is enlarged to a level that allows training and testing of such algorithms.

On the other hand, a deep learning approach could be used for both feature detection and classification. An entire segmented PRM could be fed to a deep neural network (DNN) or convolutional neural network (CNN) which could potentially classify both the state of the muscle (damaged and undamaged) and the type of trauma that affected the muscle. For this scenario, only the database of segmented PRMs has to be increased.

## CONCLUSIONS

In this study, we used ME, Shannon's entropy and shape parameter values based on log-compressed B-mode images to assess the state of the PRM in two scenarios: at rest and in maximum contraction. The results indicate that the shape parameter of the first-order statistics of the speckle (gray value distribution) is the strongest parameter for distinguishing intact and damaged PRMs. This was determined by analyzing the AUC. Entropy as a parameter had a slightly less strong performance. Also, analysis of the muscle in contraction has decreased performance with respect to analysis at rest. This supports the hypothesis that a change in the state of the tissue will result in a change in the statistical distribution of gray values in a B-mode image of the PRM.

## DECLARATION OF COMPETING INTEREST

The authors declare no conflicts of interest in this work.

**Acknowledgments**—This research is supported by the project Gynecological Imaging using 3D Ultrasound (GYNIUS) (Project No. 15301) from the Netherlands Organization for Scientific Research (NWO).

We thank Philips Healthcare (Bothell, WA, USA) for providing us the EPIQ 7G US system for data acquisition as well as the license for the proprietary software QLAB (Philips Healthcare, Andover, MA, USA) for data conversion.

## SUPPLEMENTARY MATERIALS

Supplementary material associated with this article can be found in the online version at [doi:10.1016/j.ultrasmedbio.2022.10.003](https://doi.org/10.1016/j.ultrasmedbio.2022.10.003).

## REFERENCES

Bedretdinova D, Fritel X, Panjo H, Ringa V. Prevalence of female urinary incontinence in the general population according to different definitions and study designs. *Eur Urol* 2016;69:256–264.

Bellos-Grob A. Structural and functional ultrasound imaging of the pelvic floor during pregnancy and postpartum. : Utrecht University; 2016 PhD thesis.

Cardillo G. ROC curve: Compute a receiver operating characteristics curve. 2021. Available at: <https://github.com/dnafinder/roc>. Accessed June 2021.

Chen JR, Chao YP, Tsai YW, Chan HJ, Wan YL, Tai DI, Tsui PH. Clinical value of information entropy compared with deep learning for ultrasound grading of hepatic steatosis. *Entropy* 2020;22:1006.

Crema MD, Yamada AF, Guermazi A, Roemer FW, Skaf AY. Imaging techniques for muscle injury in sports medicine and clinical relevance. *Curr Rev Musculoskelet Med* 2015;8:154–161.

Das S, Hansen HH, Hendriks GA, van den Noort F, Manzini C, van der Vaart CH, de Korte CL. 3D ultrasound strain imaging of puborectalis muscle. *Ultrasound Med Biol* 2021;47:569–581.

de Araujo CC, Coelho AS, Stahlschmidt P, Juliato CRT. Does vaginal delivery cause more damage to the pelvic floor than cesarean section as determined by 3D ultrasound evaluation? A systematic review. *Int Urogynecol* 2018;29:639–645.

DeLancey J. Pelvic floor anatomy and pathology. In: Hoyte L, Damaser MS, (eds). *Biomechanics of the female pelvic floor*. London: Academic Press; 2016. p. 13–51.

Dieter AA, Wilkins MF, Wu JM. Epidemiological trends and future care needs for pelvic floor disorders. *Curr Opin Obstet Gynecol* 2015;27:380.

Dietz HP. Pelvic floor muscle trauma. *Expert Rev Obstet Gynecol* 2010;5:479–492.

Dietz HP. Pelvic floor trauma in childbirth. *Australian NZ J Obstet Gynaecol* 2013;53:220–230.

Gdynia HJ, Müller HP, Ludolph AC, Köninger H, Huber R. Quantitative muscle ultrasound in neuromuscular disorders using the parameters 'intensity', 'entropy', and 'fractal dimension'. *Eur J Neurol* 2009;16:1151–1158.

Gijsbertse K, Sprengers A, Nillesen M, Hansen H, Lopata R, Verdonchot N, de Korte C. Three-dimensional ultrasound strain imaging of skeletal muscles. *Phys Med Biol* 2017;62:596–611.

Girardi A. Assessment of ultrasonic tissue characterization. Master's thesis. University of Twente, 2019.

Grob ATM, Hitschrich N, van de Waarsburg MK, Withagen MIJ, Schweitzer KJ, van der Vaart CH. Changes in global strain of puborectalis muscle during pregnancy and postpartum. *Ultrasound Obstet Gynecol* 2018;51:537–542.

Hendriks GAGM, Holländer B, Menssen J, Milkowski A, Hansen HHG, de Korte CL. Automated 3D ultrasound elastography of the breast: A phantom validation study. *Phys Med Biol* 2016;61:2665–2679.

Holland MR, Lewis SH, Hall CS, Finch-Johnston AE, Handley SM, Wallace KD, D'Sa AP, Prater DM, Pérez JE, Miller JG. Effects of tissue anisotropy on the spectral characteristics of ultrasonic backscatter measured with a clinical imaging system. *Ultrason Imaging* 1998;20:178–190.

Manzini C, van den Noort F, Grob ATM, Withagen MIJ, Slump CH, van der Vaart CH. Appearance of the levator ani muscle subdivisions on 3D transperineal ultrasound. *Insights Imaging* 2021;12:1–8.

Mase GT, Smelser RE, Mase GE. *Continuum mechanics for engineers*. Boca Raton FL: CRC Press; 2010.

Rijsterborgh H, Mastik F, Lancée CT, Van Der Steen AFW, Sassen LMA, Verdouw PD, Roelandt J, Bom N. Ultrasonic myocardial integrated backscatter and myocardial wall thickness in animal experiments. *Ultrasound Med Biol* 1990;16:29–36.

Sikdar S, Diao G, Turo D, Stanley CJ, Sharma A, Chambliss A, Laughrey L, Aralar A, Damiano DL. Quantification of muscle tissue properties by modeling the statistics of ultrasound image intensities using a mixture of gamma distributions in children with and without cerebral palsy. *J Ultrasound Med* 2018;37:2157–2169.

Silva E, Parente M, Jorge RN, Mascarenhas T. Characterization of the biomechanical properties of the pubovisceral muscle of two women—one with pelvic organ prolapse and other without pathology. 2017 IEEE 5th Portuguese Meeting on Bioengineering (ENBENG). New York: IEEE; 2017. p. 1–4.

Svabik K, Shek K, Dietz H. How much does the levator hiatus have to stretch during childbirth?. *BJOG* 2009;116:1657–1662.

Thijssen JM, Starke A, Weijers G, Haudum A, Herzog K, Wohlsein P, Rehage J, de Korte CL. Computer-aided B-mode ultrasound

- diagnosis of hepatic steatosis: A feasibility study. *IEEE Trans Ultrason Ferroelectr Freq Control* 2008;55:1343–154.
- Tsui PH, Hsu CW, Ho MC, Chen YS, Lin JJ, Chien L, Chu CC. Three-dimensional ultrasonic Nakagami imaging for tissue characterization. *Phys Med Biol* 2010;55:5849–5866.
- van de Waarsenburg MK, van der Vaart CH, Withagen MIJ. Structural changes in puborectalis muscle after vaginal delivery. *Ultrasound Obstet Gynecol* 2019;53:256–261.
- van den Noort F, Grob A, Slump C, van der Vaart C, van Stralen M. Automatic segmentation of puborectalis muscle on three-dimensional transperineal ultrasound. *Ultrasound Obstet Gynecol* 2018;52:97–102.
- van Holsbeeck MT, Introcaso JH. *Ultrasound*. Philadelphia: Mosby Press; 2001.
- van Hooren B, Teratsias P, Hodson-Tole EF. Ultrasound imaging to assess skeletal muscle architecture during movements: A systematic review of methods, reliability, and challenges. *J Appl Physiol* 2020;128:978–999.
- Weijers G, Starke A, Thijssen JM, Haudum A, Wohlsein P, Rehage J, de Korte CL. Transcutaneous vs. intraoperative quantitative ultrasound for staging bovine hepatic steatosis. *Ultrasound Med Biol* 2012;38:1404–1413.
- Weijers G, Wanten G, Thijssen JM, van der Graaf M, de Korte CL. Quantitative ultrasound for staging of hepatic steatosis in patients on home parenteral nutrition validated with magnetic resonance spectroscopy: A feasibility study. *Ultrasound Med Biol* 2016;42:637–644.
- Weng WC, Tsui PH, Lin CW, Lu CH, Lin CY, Shieh JY, Lu FL, Ee TW, Wu KW, Lee WT. Evaluation of muscular changes by ultrasound Nakagami imaging in Duchenne muscular dystrophy. *Sci Rep* 2017;7:4429.
- Whittaker JL, Stokes M. Ultrasound imaging and muscle function. *J Orthop Sports Phys Ther* 2011;41:572–580.
- Woodhouse JB, McNally EG. Ultrasound of skeletal muscle injury: An update. *Semin Ultrasound CT MRI* 2011;32:91–100.
- Zijta FM, Froeling M, Nederveen AJ, Stoker J. Diffusion tensor imaging and fiber tractography for the visualization of the female pelvic floor. *Clin Anat* 2013;26:110–114.